

# Time dependent forcing in the Swift– Hohenberg equation

Punit Gandhi,<sup>1,\*</sup> Cédric Beaume,<sup>1</sup> and Edgar Knobloch<sup>1,†</sup>

<sup>1</sup>*Department of Physics, University of California, Berkeley CA 94720, USA*

(Dated: April 16, 2014)

## Abstract

The subcritical Swift– Hohenberg equation has a stable periodic solution for sufficiently strong forcing which does not exist for a weak linear forcing. When the bifurcation creating this solution from the trivial state is subcritical, there also exists a region of bistability where both the periodic state and the trivial state coexist and are stable. A pinning region is formed within the region of bistability where an infinite snake of stable localized solutions exist in addition to the periodic and trivial states. We add a time-periodic forcing to the Swift Hohenberg equation that takes the system between these regions of parameter space. For specific values of the frequency, amplitude, and center of the periodic forcing, we (hopefully) find something interesting.

---

\* punit.gandhi@berkeley.edu

† knobloch@berkeley.edu

## I. INTRODUCTION

The Swift–Hohenberg equation [1] (SHE) serves as a model for pattern formation in a broad range of physical systems []. The existence, structure, and stability of localized solutions within the SHE has been studied in great detail [2–4]. This equation, which takes the form

$$u_t = ru - (1 + \partial_x^2)^2 u + N[u], \quad (1)$$

describes the dynamics of a real field  $u$  over one spatial dimension in time, where  $N$  is some nonlinear function of  $u$ . We have rescaled the equation so that the critical wavenumber that defines the natural wavelength of the patterned state is unity. We will be interested in two possible choices of  $N$ , namely  $N_{23}[u] = bu^2 - u^3$  and  $N_{35}[u] = bu^3 - u^5$ . The strength of the linear forcing term  $r$  and the strength of the quadratic/cubic nonlinearity  $b$  are left as parameters of the system.

We consider the case when the forcing is no longer constant in time, namely  $r \rightarrow r_0 + \rho \sin \omega t$ . Pattern formation in ecological systems that are periodically forced by the seasons or the daily variations in insolar flux are one example of a physical motivation for considering this kind of system []. Other physical systems that might be described by such a periodically forced model include ... []. Furthermore, oscillations that effectively create and destroy attractors have been shown to produce new “ghost” attractors that do not exist in the time-independent system for any value of the parameter []. While this has been done for the case of simple oscillators, the present work provides an extension of these observations to higher dimensions.

We first recount the relevant details of the original Swift-Hohenberg equation before discussing some numerical results of the time-dependent forced case. Hopefully we will also eventually add a section describing some theoretical understanding of the results we obtained. Note that all the work done so far is for the  $N_{23}$  nonlinearity and  $b = 1.8$ .

## II. BISTABILITY AND LOCALIZED SOLUTIONS IN SHE

Here we will describe the structure of the steady-state solutions of SHE near the bifurcation that creates the periodic state. We will focus on the case when the nonlin-

earity parameter  $b$  creates these states in a subcritical bifurcation from the trivial state at  $r = 0$ . A bifurcation diagram of the steady state solutions (Fig. 1, from J. Burke et al) shows the trivial state, the periodic state, and localized solution branches.

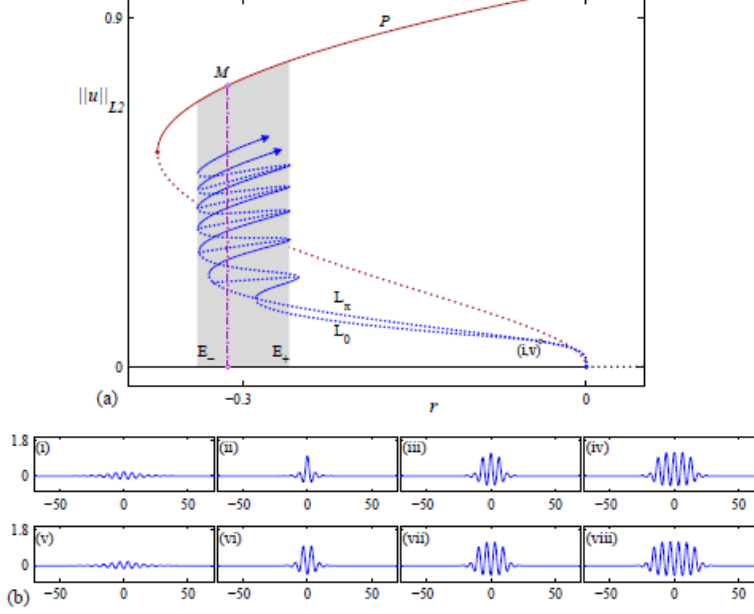


FIG. 1: This figure was taken from Burke[] (a) Bifurcation diagram showing the snakes-and-ladders structure of localized states. Away from the origin the snaking branches  $L_0$  and  $L_-$  are contained within the snaking region (shaded) between  $E_-$  and  $E_+$ , where  $r(E_-) \approx -0.3390$  and  $r(E_+) \approx -0.2593$ . Solid (dotted) lines indicate stable (unstable) states. In addition, the Maxwell point  $M$ , occurring at  $r(M) \approx -0.3128$  is indicated with a vertical dash-dot line. The saddle node bifurcation that creates the stable periodic state occurs at  $r < r(SN_P) \approx -0.3744$ , defining the left edge of the bistability region. We will also find it useful to define the center of the snaking region  $C$ , which corresponds to the forcing parameter  $r(C) \approx -0.2992$ . (b) Sample localized profiles  $u(x) : (i - iv)$  lie on  $L_0$ , near onset and at the 1st, 3rd, and 5th saddle-nodes from the bottom, respectively; (v-viii) lie on  $L_-$ , near onset and at the 1st, 3rd, and 5th saddle-nodes, respectively. Parameters:  $b = 1.8$ .

We see that the trivial solution is stable for  $r < 0$ , and becomes unstable as as the

periodic solution is created through a bifurcation at  $r = 0$ . As we are looking at the subcritical case, we see a saddle-node bifurcation of the periodic branch where it gains stability at  $SN_P$ . Thus we have only a stable trivial solution for  $r < r(SN_P) \approx -0.3744$ . At this point, a stable periodic solution is created but is energetically unfavorable to the trivial state. For  $r(E_-) < r < r(E_+)$ , we have a zoo of localized solutions (including an entire sequence of stable localized solutions on each snaking branch) that exist in addition to the stable trivial and periodic solutions. We note that within this region,  $r(M)$  indicates the transition from the trivial state being energetically favorable to the periodic state becoming energetically favorable. We will also find it useful to define the center of the snaking region  $C$ , which corresponds to the forcing parameter  $r(C) \approx -0.2992$ . Between  $r(E_+)$  and  $r = 0$ , we again have only the periodic solution and the trivial solution as stable but with the periodic solution now more energetically favorable. Finally, for  $r > 0$ , the trivial solution loses stability and only the periodic solution remains as stable. We note that other stable solutions exist (e.g. the flat, nonzero solutions created at the transcritical bifurcation at  $r = 1$ ) but that they do not play a role in our region of interest with our current choice of parameters (e.g.  $b = 1.8$ ).

In addition to understanding the structure of the stationary solutions, it will also be helpful to understand what is known about the dynamics of the localized solutions when the system is pushed just outside of the snaking region. Burke and Knobloch [2] have shown that near the snaking region (e.g. for  $r = r(E_{\pm}) \pm \delta$  where  $\delta \ll 1$ ), a localized solution will move towards the more energetically favorable of the trivial and the periodic state. Above the snaking region, for example, a localized solution will nucleate periods of the pattern in quick bursts with some longer transition time  $T \propto \delta^{-1/2}$  in between each nucleation event.

### III. NUMERICAL METHODS

All simulations in time used periodic boundary conditions and a domain of  $80\pi$  (e.g. 40 characteristic wavelengths). A 4th order exponential time differencing scheme[5] was used to step forward in time while spectral methods on a grid of 1024 points were used for the spatial calculations. Steady state solutions were computed by numerical

continuation using AUTO [6]. We will focus on SHE23 case with  $b = 1.8$  and will always initialize the problem with a localized solution that is stable for the constant forcing ( $\rho = 0$ ) case with the given choice of  $r_0$ . We can vary the way the forcing oscillates ( $r \rightarrow r_0 + \rho \sin \omega t$ ) in 3 ways: (1) the amplitude of the oscillation,  $\rho$  (2) the point about which the oscillation occurs,  $r_0$  (3) the frequency with which the oscillation occurs,  $\omega$ .

#### IV. FRONT SPEED JUST OUTSIDE OF THE PINNING REGION

##### A. constant forcing

Burke and Knobloch [2] have shown that near the snaking region (e.g. for  $r = r(E_{\pm}) \pm \delta$  where  $\delta \ll 1$ ), a localized solution will move towards the more energetically favorable of the trivial and the periodic state. A numerical example of this on a domain of 40 periods of the characteristic wavelength is shown in Fig. 2. A localized solution that is stable for  $r \approx 0.2944$  is initialized above the snaking region (e.g.  $r = 0.2$ ) and allowed to grow until it fills the domain. We note that it grows to a solution containing 39 periods, and a corresponding numerical continuation calculation produces a snaking branch of steady state solutions that emerges as a secondary bifurcation from a 40 period solution but reconnects to a 39 period solution. This phenomenon has been explained [7] in terms of the Eckhaus instability for the case of the steady state solutions. We can see from Fig. 2 that the time from one nucleation event to the next is approximately 18, though the last nucleation event seems to take a bit longer. As the transition time  $T$  for this case is on the same order as the time over which the nucleation event occurs, we have likely reached the limit of applicability of the theory described above.

We show the results of simulations for our parameters (Fig. 3) to numerically confirm the  $T_{nuc} \propto \delta^{-1/2}$  law and locate the region of validity. We also show a graph of the front speed (calculated as  $2\pi/T_{nuc}$ ) as a function of  $r_0$  for the constant forcing case. It is clear from these graphs, that the front moves faster to the left of pinning region in the parameter regime we are looking at. We also note that beyond  $\delta$  of about 0.036, our algorithm fails to distinguish nucleation events to the left of the pinning region because

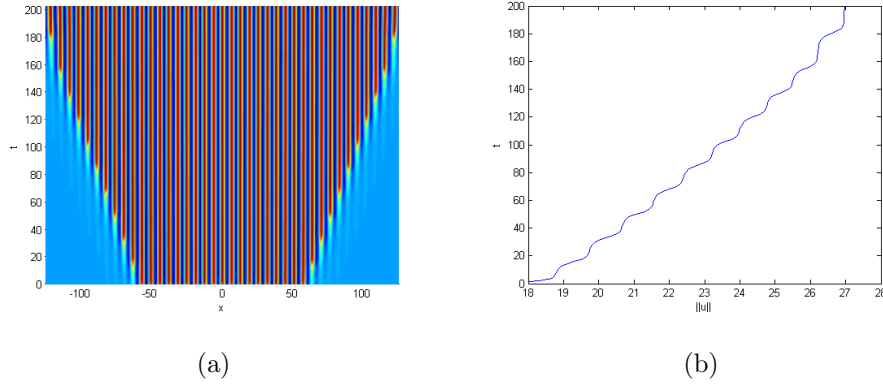


FIG. 2: A simulation of the SHE with  $N_{23}$ ,  $b = 1.8$  and  $r = -0.20$  (e.g.  $\delta \approx 0.06$ ) is initialized using a localized solution that is stable within the snaking region (e.g. at  $r = -0.2944$ ). The solution growing in time (a) with red as high values and blue as low values. The norm of the solution as it grows in time is shown in (b).

they are no longer clearly separated by a period of slow change in the solution. With an amplitude of oscillation of  $\rho = 0.1$ , the system actually reaches above this cutoff for most of the  $r_0$  values we scan over.

We also calculated the cost to nucleate a period on each end of the solution in terms of free energy as a function of the forcing parameter for localized solutions within the pinning region. The free energy is defined by

$$F[u] = -\frac{1}{\Gamma} \int_{\Gamma} \frac{1}{2} r u^2 - \frac{1}{2} [(1 + \partial_x^2)u]^2 + \frac{1}{3} b u^3 - \frac{1}{4} u^4 dx \quad (2)$$

where  $\Gamma$  defines the domain of  $u$ .

## B. small oscillations

We include some preliminary results on how small oscillations affect the time between nucleation events for the case when a localized structure grows outside of the pinning region. We take  $\rho = 5 \times 10^{-3}$ , and initialize the simulation with a localized solution of five periods that is stable at the right edge of the pinning region. We compare the average time between nucleation events to the constant forcing case (Fig. 5, which follows the  $T_{osc} \propto \delta^{-1/2}$ ).

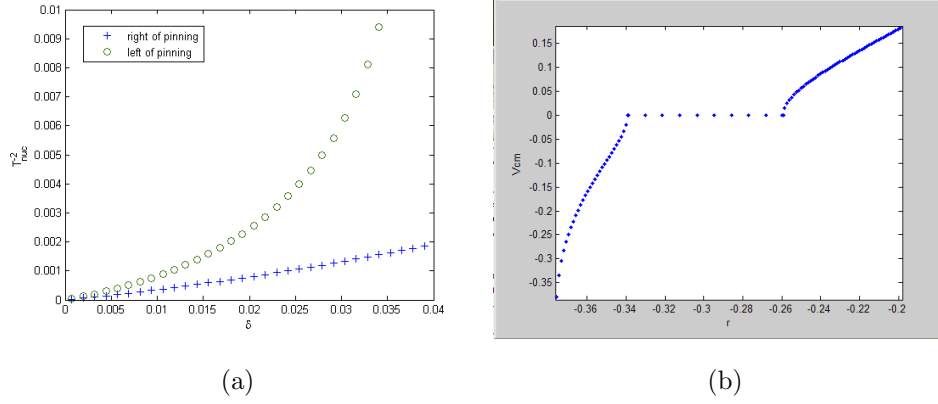


FIG. 3: Simulation of the SHE with  $N_{23}$  with  $b = 1.8$  show (a)  $1/T_{nuc}^2$ , where  $T_{nuc}$  is the time between nucleation/decay events, as a function of distance from the edge of the pinning region, and (b) the front speed as a function of the forcing parameter. We note that the initial solution used in these simulations was on a saddle node bifurcation of snaking branch at the closest edge of the pinning region.

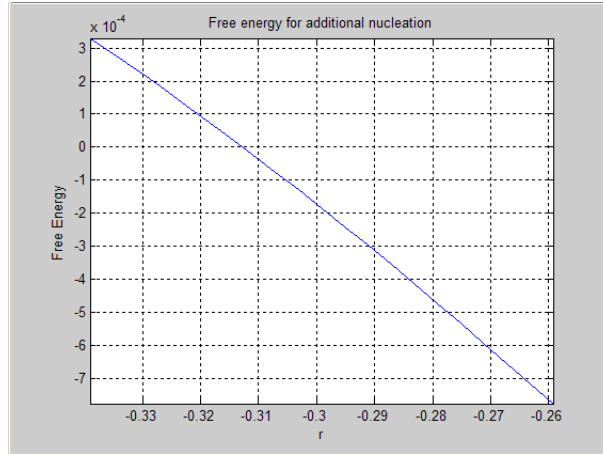


FIG. 4: The difference in free energy between stable localized solutions that differ by 2 periods as a function of the forcing parameter  $r$ .

## V. SMALL OSCILLATIONS WITHIN THE PINNING REGION

The phase space of this problem is infinite dimensional, but can choose a two dimensional slice of the max value vs L2 norm of  $u$  to help us visualize trajectories in time. All the plots will also contain the periodic and snaking branch of the time steady

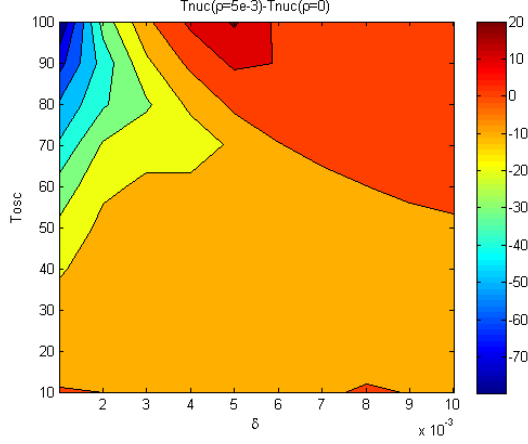


FIG. 5: difference in time between nucleation events for the  $\rho = 5 \times 10^{-3}$  case and the constant forcing case ( $\rho = 0$ ).

solutions (Fig. 6) as reference.

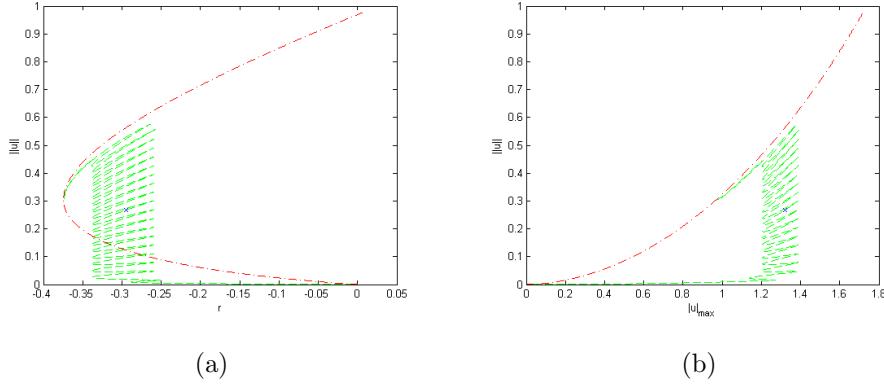


FIG. 6: (a) A plot of the time-steady localized (green dash) and periodic (red dash-dot) solutions as a function of the forcing parameter in the problem with constant  $r$  in time. The blue x indicates the localized initial solution for the simulations with time-periodic forcing. We note that future plots will zoom into the region near this x. (b) This same data is plotted in terms of the max value vs L2 norm of the solutions in order to provide some reference for the trajectories of the time-dependent parameter case.

We first oscillate the forcing about the Maxwell point within the snaking region



( $r_0 = -0.3128$  and  $\rho = 0.025$ ) for various frequencies (Fig. 7). An oscillation period of 500 is sufficiently slow that the trajectory nearly follows the time-independent snaking region. At a period of 5 and 0.5, we see that the solution may be approaching a steady orbit in time but more detailed simulations should be done here. It may be that the oscillations are fast enough at a period of 5 or 0.5 to attempt some averaging techniques to build a theory for this parameter regime. We note that the time scale on which the nucleation process occurs is 10.

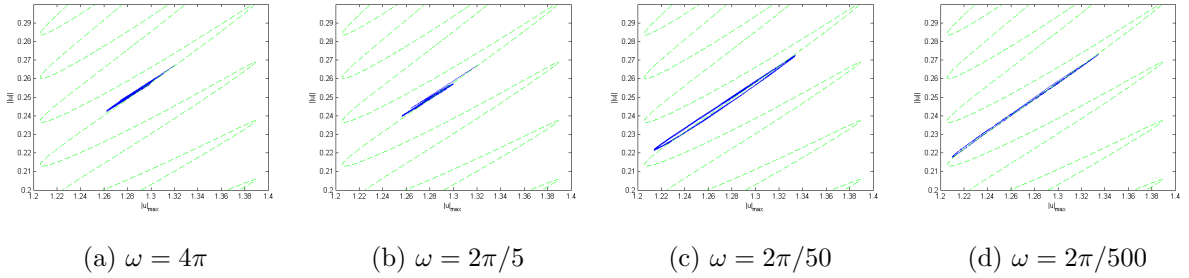


FIG. 7: Oscillations of the forcing parameter about the Maxwell point within the snaking region. The forcing parameter as a function of time is given by  $r \rightarrow -0.3128 + 0.025 \sin \omega t$  for various values of  $\omega$  (a)-(d). Note that these figures are plotting the maximum value of the solution vs. its L2 norm just as in Fig. 6 except that they are zoomed into a smaller region of the phase space slice centered around the initial condition (the blue x). The time-independent snaking branch is also shown here for reference.

## VI. LARGE OSCILLATIONS EXTENDING BEYOND THE SNAKING REGION

### A. Dependence on oscillation period

We can now increase the amplitude of oscillation to take the system in and out of the snaking region. With an amplitude of  $\rho = 0.1$  and a frequency of  $2\pi/50$ , simulations indicate a stable region of  $r$  where one period is added and decays at each front during

one cycle but there is no net motion. For  $-0.290 \leq r_0 \leq -0.285$  the solution “breathes” by one period at each front, but is stable. For  $r_0 \leq -0.295$ , in addition to breathing, periods of the solution decay overall from the solution over the course of many cycles. For  $r_0 \geq -0.280$ , periods are nucleated on average.

If we increase the oscillation period to 100, we see the region of stable breathing is shifted to slightly higher values of  $r_0$  – stable at  $r_0 = -0.285$ ,  $-0.280$  and the breathing involves the nucleation and decay of two periods on each front. At an oscillation period of 200, the region of stable breathing presumably occurs between  $r_0 = -0.28$  and  $r_0 = -0.275$ , but is smaller than  $5 \times 10^{-3}$ . The localized pattern nucleates and decays 4 periods within each cycle. Further simulations could be done to put tighter bounds on these regions, and to ensure that there is no motion of the fronts over many cycles (all simulations here were run for 1000 units of time). Results from the simulations are shown at the different oscillation frequencies for  $r_0 = -0.28$  in Fig. 8. We see the localized structure grow when the period is 50, remain stable when the period is 100, and decay when the period is 200. It is interesting to note from these figures that oscillations in amplitude of the periods at the front are out of phase from the rest of the localized structure.

For all three oscillation frequency values explored at with this amplitude, there exist oscillations of the forcing centered about values of  $r_0$  greater than the center of the snaking region (and the Maxwell point) that cause the solution to decay. In these cases, the decay happens even though the forcing spends more time above the snaking region where the solution would be expected to grow than below it. This seems to imply that the trivial state is more strongly attracting to the left of the snaking region than the periodic state is to the right of the snaking region. Maybe this has to do with the choice of initial condition, or with the fact that the amplitude chosen takes the system outside of the region on of bistability below the snaking region, but not above. Similar simulations with  $\rho = 0.6$  so that the oscillations remain entirely within the region of bistability, so a stable breathing solution with an oscillation period of 100 about  $r_0 = -0.295$ . Thus the stable region in parameter space is still to the right of the center of the snaking region. We would like to note that the region of stable breathing in the simulations did not depend on the phase of the oscillation (e.g. if the forcing

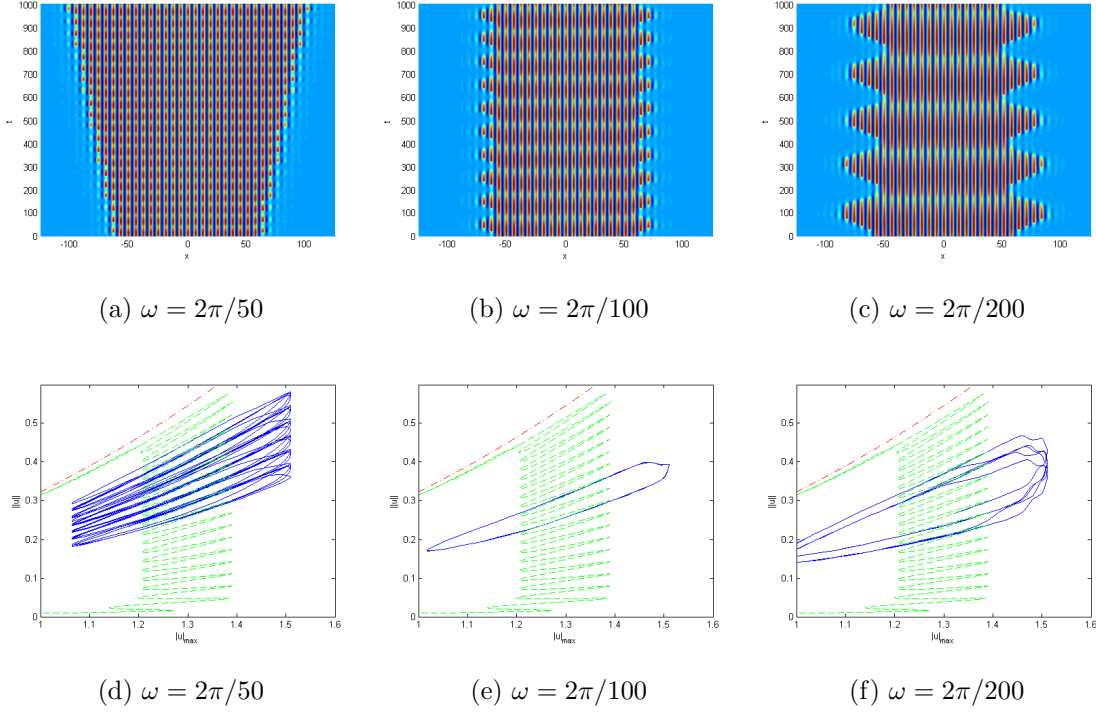


FIG. 8: Oscillations of the forcing parameter in and out of the snaking region. The forcing parameter as a function of time is given by  $r \rightarrow -0.28 + 0.1 \sin \omega t$  for various values of  $\omega$ . (a)-(c) show the solution as a function of time and (d)-(f) show the corresponding trajectories along the max value - L2 norm phase space slice (the time-independent snaking branch and periodic branches are also shown here for reference).

parameter increased first or decreased first).

Figure 9 show some results from a scan of the parameter space over the period of oscillation  $T_{osc}$ , and the average value of forcing  $r_0$  with a fixed amplitude of oscillation,  $\rho = 0.1$ . We track the front of solution in terms of its first moment:

$$X_{cm} = \frac{1}{||u||} \int_{L/2}^{L/2} |x| |u|^2 dx \quad (3)$$

where

$$||u|| = \int_{L/2}^{L/2} |u|^2 dx \quad (4)$$

This give half the distance from the center of the domain to the edge of a localized

solution. The speed is then defined by  $V_{cm} = dX_{cm}/dt$ , and is really half the speed of the front.

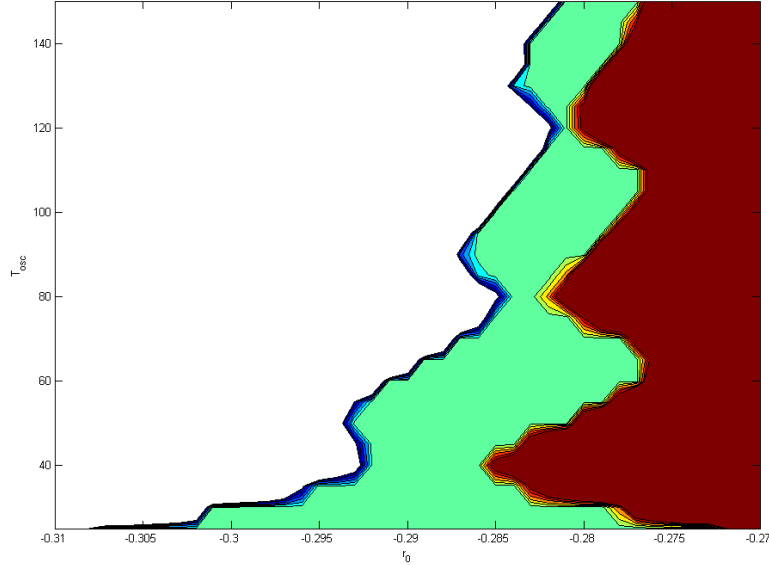


FIG. 9: The average speed at which the solution grows or decays as a function of oscillation period and oscillation center of the forcing parameter when  $\rho = 0.1$ . The solution had decayed by 6 or more periods over the course of the simulation (2000 units of time) in the white region, and has grown by six or more periods over the course of the simulation in the red region. The green region indicates where the solution has not grown or decayed on average.

We note that changing the phase of the oscillation in the forcing (e.g.  $\rho \rightarrow -\rho$ ) does not seem to affect the stable region in this graph, but we need to do more work to confirm this is the case. In order to explore the small scale bumpiness, we have zoomed in to a smaller region of parameter space with a finer mesh. The results are shown in Fig. 10. We suspect that this bumpiness is due to the representation and grid approximation, and are working to smooth it out.

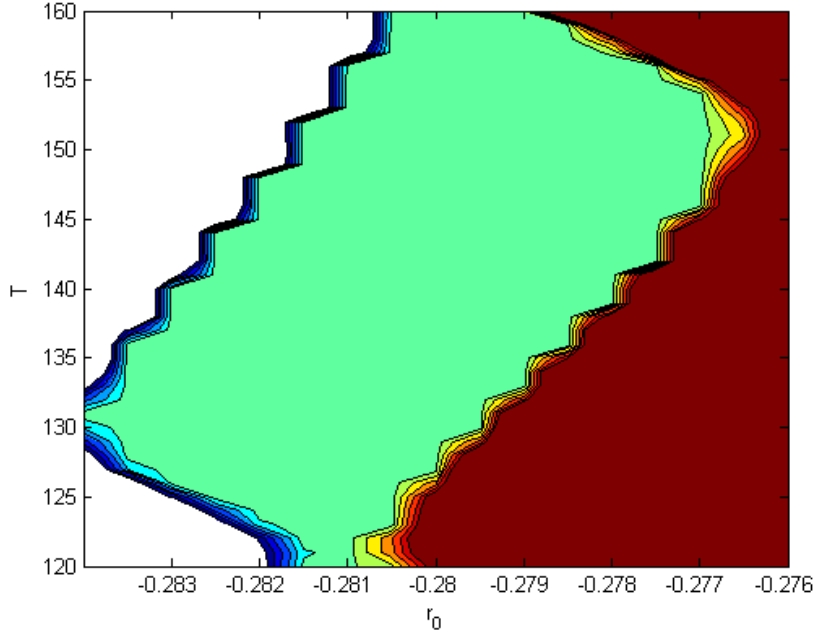


FIG. 10: The average speed at which the solution grows or decays as a function of oscillation period and oscillation center of the forcing parameter. The solution had decayed by 6 or more periods over the course of the simulation (2000 units of time) in the white region, and has grown by six or more periods over the course of the simulation in the red region. The green region indicates where the solution has not grown or decayed on average.

### B. Dependence on oscillation amplitude

We have also done preliminary calculations on  $\rho = 0.06$  and  $\rho = 0.08$  (shown in Fig. 11), and have found that decreasing  $\rho$  seems to stretch graph out vertically so that you need a longer period to see the same qualitative features. This makes sense given that a smaller oscillation amplitude means less time outside of the snaking region.

We note that our data on the front speed shown in Fig. 3 stretches far enough to cover all of the forcing parameters that are sampled during the simulations for the  $\rho = 0.06$  case. Given the speed of the front as a function of the forcing parameter,  $V_0(r)$ , We numerically determine a “break-even” point were we would not expect the front to move on average for a particular value of  $r_0$ . We define  $r_*$  by the condition

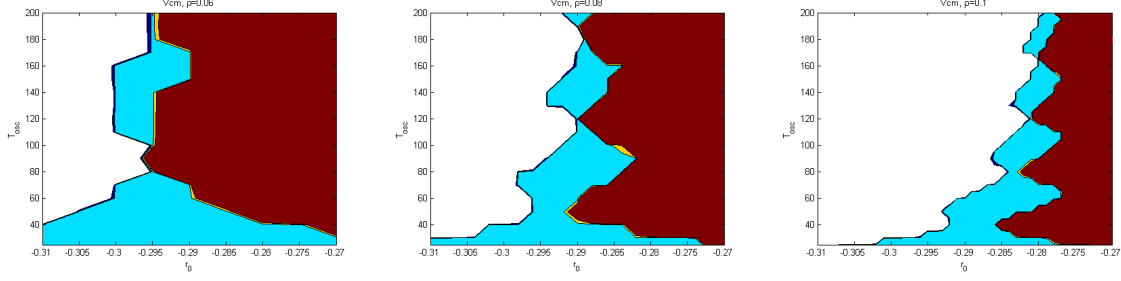


FIG. 11: The average speed at which the solution grows or decays as a function of oscillation period and oscillation center of the forcing parameter when (a)  $\rho = 0.06$ , (b)  $\rho = 0.08$ , (c)  $\rho = 0.1$ . The solution had decayed by 6 or more periods over the course of the simulation (2000 units of time) in the white region, and has grown by six or more periods over the course of the simulation in the red region. The green region indicates where the solution has not grown or decayed on average.

that

$$\int_0^{2\pi} V_0(r_* + \rho \sin \phi) d\phi = 0. \quad (5)$$

For  $\rho = 0.06$ , we find that  $r_* \approx -0.295$ , which roughly corresponds to the center point of the stable region of Fig. 11.

We can also see a similar structure the region of stable oscillations if we fix the oscillation period ( $T_{osc} = 100$  shown in Fig. 12) and vary the oscillation amplitude. Note that the width of the pinning region is approximately  $\Delta r \approx .08$ .

### C. Visualizing the dynamics of the oscillations extending beyond the snaking region

In an attempt to provide some context to the results in the we define the “oscillating Maxwell point” in the oscillation center  $r_0$  where the average free energy along an oscillation of solution that is stable in time and periodic in space equals the free energy of the trivial solution (e.g. zero). For the parameter  $\rho = 0.1$ , we find this value to be shifted to the left by about 0.5 from the Maxwell point of the constant forcing case to  $r_* \approx -0.318$  (Fig. 13). The average free energy of oscillation does not have a strong dependence on the oscillation frequency, except that the stable oscillating solution

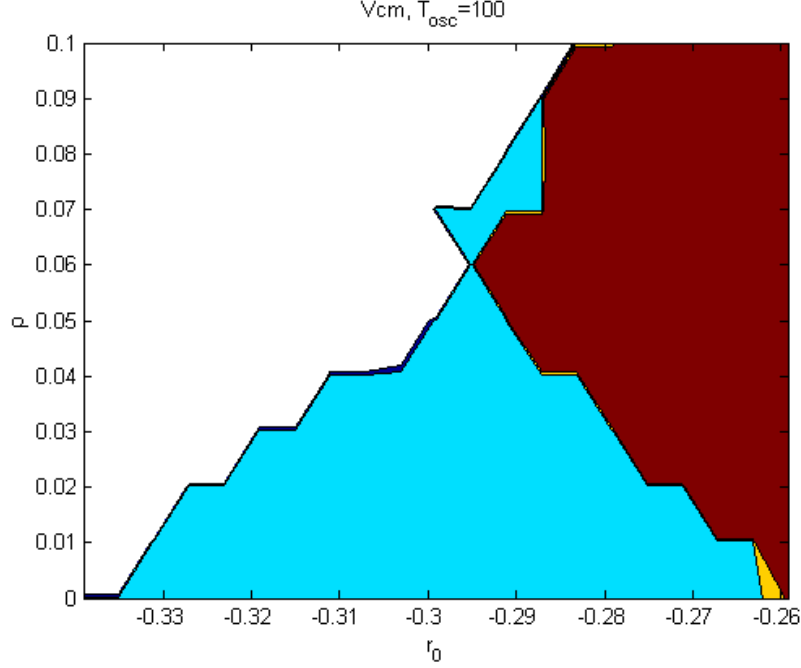


FIG. 12: The average speed at which the solution grows or decays as a function of oscillation amplitude and oscillation center of the forcing parameter when  $T_{osc} = 100$ .

The solution had decayed by 6 or more periods over the course of the simulation (2000 units of time) in the white region, and has grown by six or more periods over the course of the simulation in the red region. The green region indicates where the solution has not grown or decayed on average.

does not exist for very slow frequencies in some cases. This is because the oscillations take the system well beyond the saddle-node where the stable periodic solution of the constant forcing case is created.

To give a better sense of what is happening, we show the solution as a function of time for a series of simulations at a fixed  $r_0 = -0.28$ ,  $\rho = 0.1$  and different oscillation periods. Figures 14 and 15 show both the solution and  $X_{cm}$  for oscillation periods  $T_{osc} = 20, 40, 60, 80$ . For these parameters, the solution oscillates between growing and stable. For larger oscillation periods ( $T_{osc} \approx 200$ ), the solution transitions to going between stable and decaying as shown in Fig. 16.

For the growing solutions, we see that the pattern of growth can occur over a different number of oscillations of the forcing and this may be related to the large scale

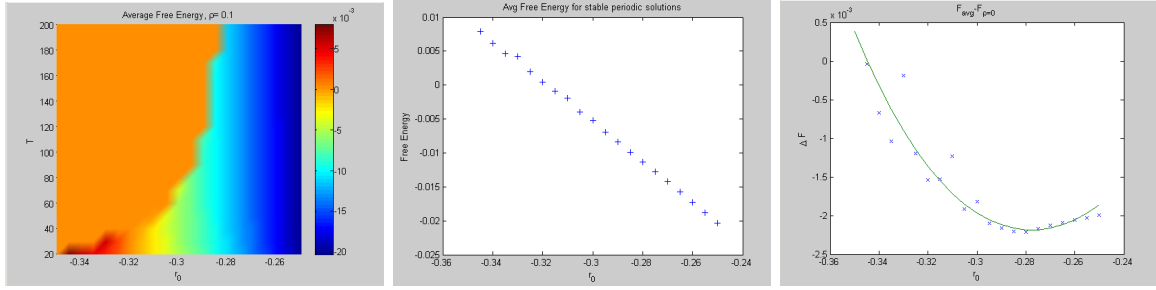


FIG. 13: (a) The average free energy along an oscillation for spatially periodic solutions that are also periodic in time under the time dependent forcing. The orange on the upper left corner indicates that the initial spatially periodic solution did not produce a stable oscillating solution in time. (b) The average free energy as a function of oscillation center for an oscillation period  $T_{osc} = 20$ . (c) The difference in free energy of the average of the oscillation and the constant forcing case. The line represents the difference of a linear fit of the average free energy from the constant forcing case.

oscillations in the boundary of the stable region shown in Fig. 9. We see, for example, a nucleation event every oscillation period at  $T_{osc} = 40$ , but two nucleation events every three oscillations in the next growing solution at  $T_{osc} = 80$ .

Figures 17 and 18 plot various phase space slices of the orbits of the stable cases detailed in the above figures in hopes of gaining some insight into the dynamics.

## VII. GROWING FROM A LOCALIZED SOLUTION TO A DOMAIN FILLING ONE

Using an oscillation with a period of 50 and centered about  $r_0 = -0.27$  and amplitude of  $\rho = 0.1$ , we can see the trajectory taken by the initial localized solution as it approaches a domain filling one (Fig. 19). The solution grows by nucleating a period on each front at each oscillation of the forcing parameter. This happens until the solution reaches 39 periods, at which point it seems to get stuck. Eventually it fills the domain with a 40 period solution. This is in contrast to the case with a constant forcing that grows into the domain with a 39 period solution.



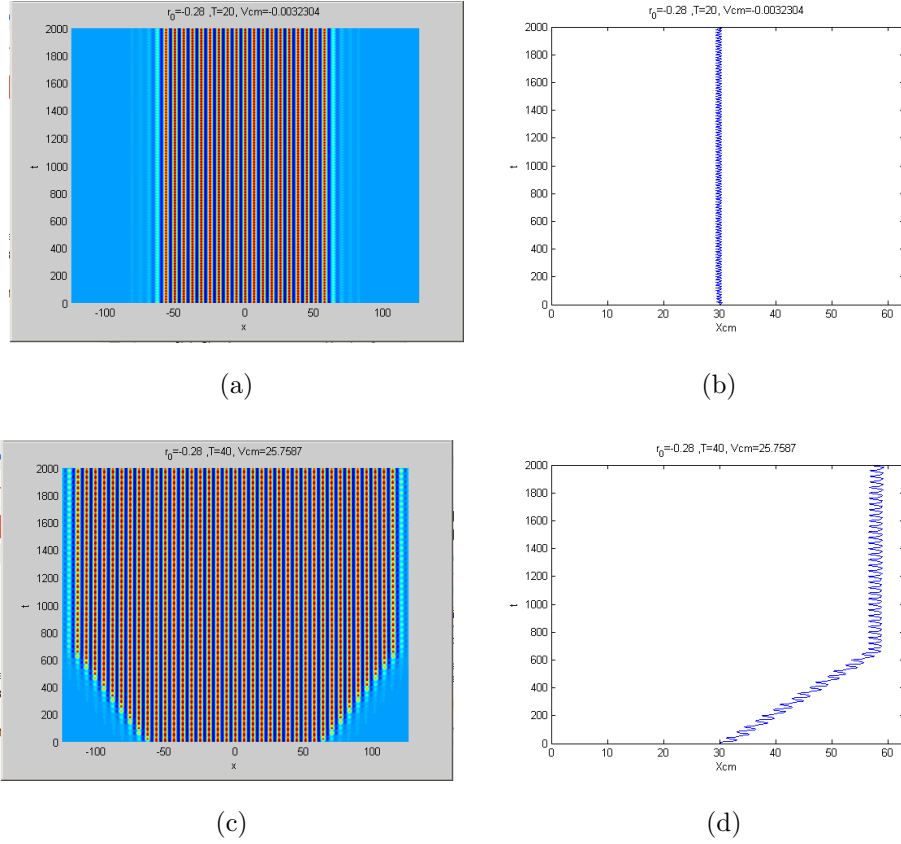
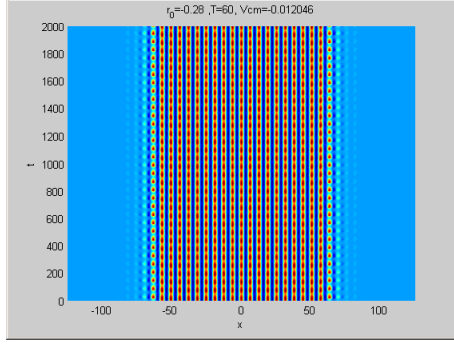
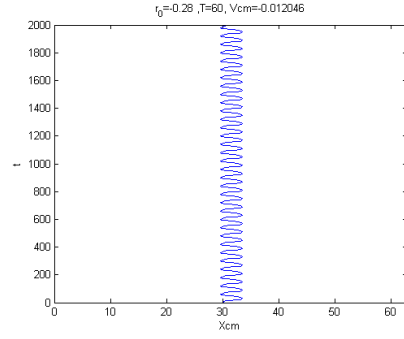


FIG. 14: Solutions along with  $X_{cm}$  are shown as function of time for a series of oscillation periods at a fixed value of  $r_0 = -0.28$ . We see that the solution oscillates between growing and stable for this region, as expected given Fig. 9. The value of  $V_{cm}$  is given in number of periods nucleated or decayed over the course of the simulation (2000 units of time), assuming no boundary.

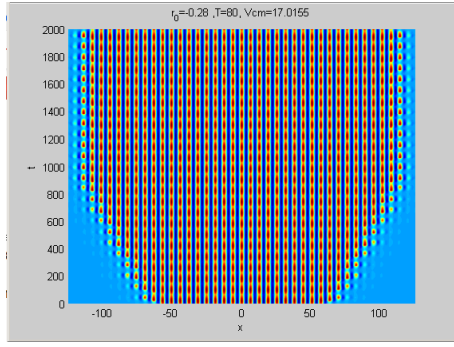
- 
- [1] J. Swift and P. C. Hohenberg, *Physical Review A* **15**, 319 (1977).
  - [2] J. Burke and E. Knobloch, *Physical Review E* **73**, 056211 (2006).
  - [3] J. Burke and E. Knobloch, *Physics Letters A* **360**, 681 (2007).
  - [4] J. Burke and E. Knobloch, *Chaos: An Interdisciplinary Journal of Nonlinear Science* **17**, 037102 (2007).
  - [5] S. Cox and P. Matthews, *Journal of Computational Physics* **176**, 430 (2002).



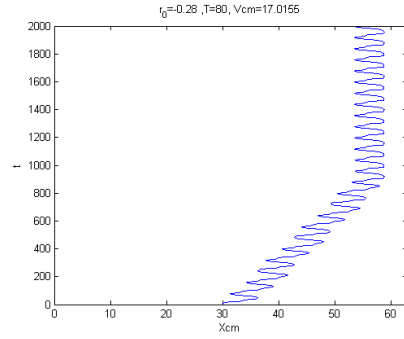
(a)



(b)



(c)

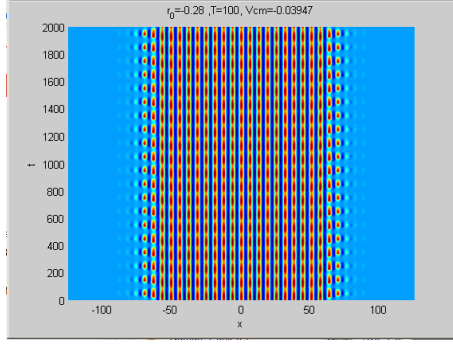


(d)

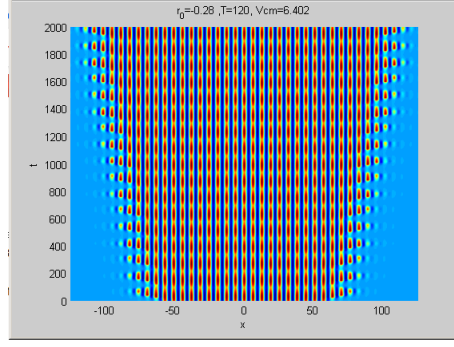
FIG. 15: Solutions along with  $X_{cm}$  are shown as function of time for a series of oscillation periods at a fixed value of  $r_0 = -0.28$ . We see that the solution oscillates between growing and stable for this region, as expected given Fig. 9. The value of  $V_{cm}$  is given in number of periods nucleated or decayed over the course of the simulation (2000 units of time), assuming no boundary.

[6] E. J. Doedel, Congr. Numer **30**, 265 (1981).

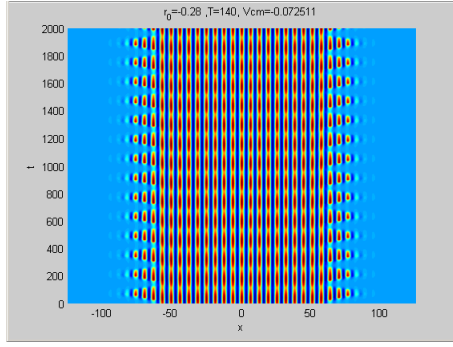
[7] A. Bergeon, J. Burke, E. Knobloch, and I. Mercader, Physical Review E **78**, 046201 (2008).



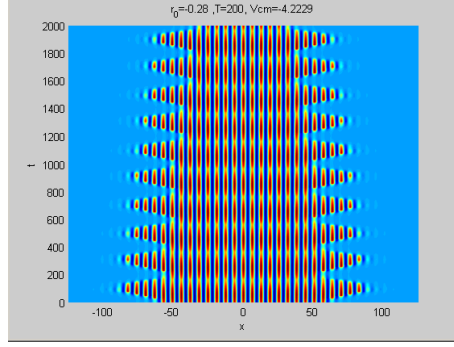
(a)



(b)



(c)



(d)

FIG. 16: The pattern of oscillating between stable and growing solution continues up to about  $T_{osc} = 140$  and then, after a longer region of stability, the solutions oscillate between stable and decaying. The value of  $V_{cm}$  is given in number of periods nucleated or decayed over the course of the simulation (2000 units of time), assuming no boundary.

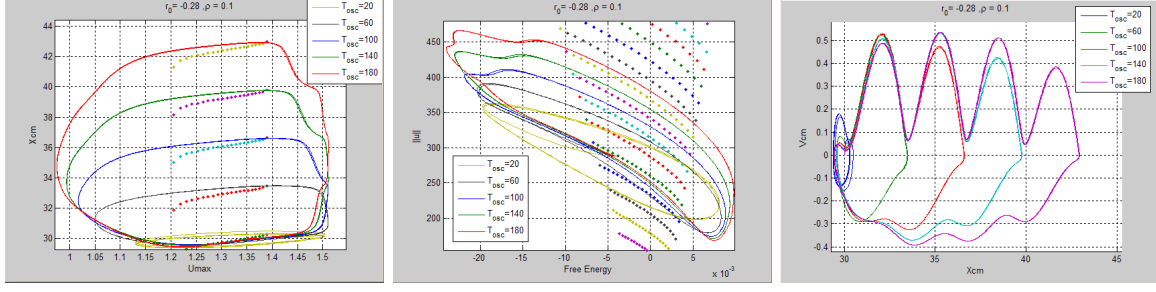


FIG. 17: (a) roughly the height vs length of the localized solution (b) roughly the size vs the energy of the solution (c) the phase space of the front

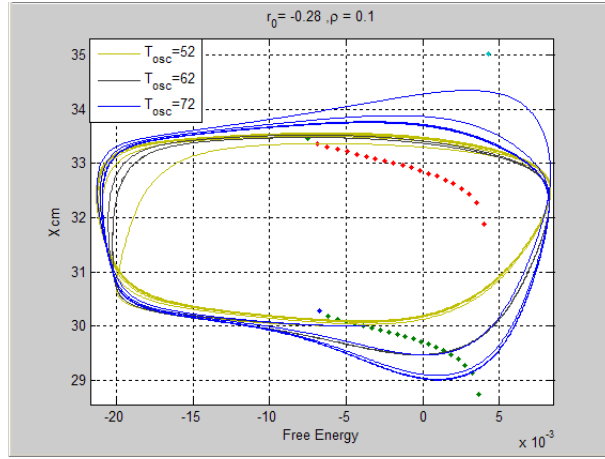


FIG. 18: Trajectories in phase space of an orbit at the edges and center of the stable region in parameter space.

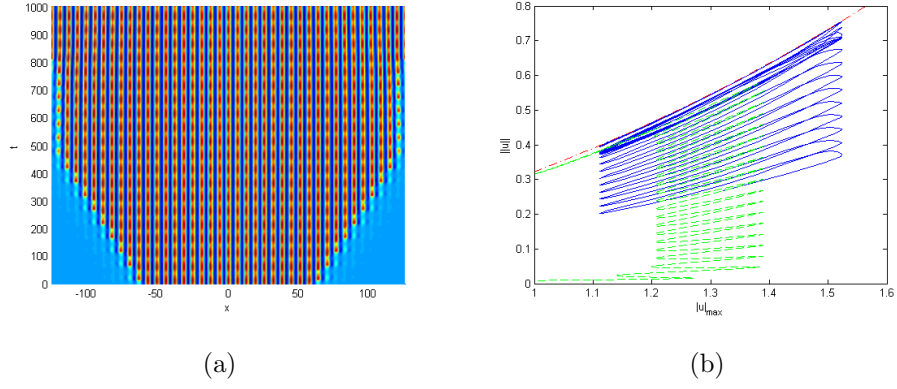


FIG. 19: Oscillations of the forcing parameter in and out of the snaking region. The forcing parameter as a function of time is given by  $r \rightarrow -0.27 + 0.1 \sin 2\pi t/50$ . The solution (a) grows in time, eventually filling the domain and the corresponding trajectory along the max value - L2 norm phase space slice (b) shows the path taken as it passes in and out of the snaking region .